J|A|C|S ARTICLES

Published on Web 09/03/2009

Determination of Structure and Phase Transition of Light Element Nanocomposites in Mesoporous Silica: Case study of NH_3BH_3 in MCM-41

Hyunjeong Kim,*,† Abhi Karkamkar,‡ Tom Autrey,*,‡ Peter Chupas,§ and Thomas Proffen†

Lujan Neutron Scattering Center, Los Alamos National Laboratory, Los Alamos, New Mexico 87545, Pacific Northwest National Laboratory, Richland, Washington 99352, and Advanced Photon Source, Argonne National Laboratory, Argonne, Illinois 60439

Received June 22, 2009; E-mail: hjkim@lanl.gov; tom.autrey@pnl.gov

Abstract: Nanocomposition of molecular crystal ammonia borane (AB) by embedding it in mesoporous silica leads to a remarkable enhancement of the hydrogen storage properties. To investigate the nature of a nanophase AB, we used atomic pair distribution function (PDF) analysis of synchrotron X-ray powder diffraction data to follow the structural evolution of AB embedded within MCM-41 at temperatures ranging from 80 to 300 K. We found that the nanophase AB residing within the mesoporous scaffold does not undergo the structural phase transition at 225 K that was observed in the neat molecular crystal. Rather, it stays in the tetragonal phase over a wide temperature range of 110 to 240 K and starts to lose structural correlation above 240 K. This finding strongly suggests that nanoconfinement of AB within mesoporous scaffolds stabilizes the high-temperature disordered tetragonal phase at a much lower temperature. PDF analyses of composite materials composed of excess AB (i.e., AB:MCM-41 > 1:1) indicates that the excess AB forms aggregates outside the mesoporous scaffold and that these aggregates have structural properties similar to neat AB, that is, the orthorhombic-to-tetragonal structural phase transition is observed at 225 K upon warming. These results may provide important insight into the mechanism behind the enhanced hydrogen storage properties of this system.

Introduction

Since the initial preparation and characterization of ordered mesoporous materials in 1992, they have been intensively used for a wide variety of chemistry applications.[1] One of the most active research areas is inclusion chemistry in which ordered mesoporous materials are used as host containers or scaffolds for organic functional groups in hybrid materials,[2] containers for nanoparticle and nanowire growth,[3] or test grounds to study the physical properties and phase transitions of adsorbates in confined spaces.[4,5] Recently, use of mesoporous materials as scaffolds for nanoconfinement of ammonia borane (AB), NH_3BH_3, was reported.[6] Such nano phase AB embedded within mesoporous silica shows dramatically enhanced hydrogen storage properties in many aspects. Undoubtedly, the determination of the structure of the guest species (i.e., AB) is an essential component for understanding the properties of such composite materials. However, the structural determination of compounds composed of light elements (i.e., soft materials) is not a trivial task when using conventional diffraction techniques. This is especially true when these soft materials are infused *inside* pores of relatively heavy mesoporous materials, because by nature, these guests inside mesoporous hosts lack long-range structural order. An emerging alternative approach is to use the atomic pair distribution function (PDF) analysis on X-ray powder diffraction data. It is not immediately obvious that X-ray is a good choice for light elements; however, currently available high-flux synchrotron X-ray sources together with area detector technology make it possible to obtain data from smaller amounts of samples over reasonably short measurement times. Statistics are sufficient to differentiate the signal of the guest species composed of light elements from that of heavy host material. This X-ray PDF approach has been applied successfully in several cases to obtain structural information of intercalated materials.[7] In this article, we demonstrate how the X-ray PDF can be used incorporating with hyperpolarized ^{129}Xe NMR data previously available to determine the structure of AB infused

† Los Alamos National Laboratory.
‡ Pacific Northwest National Laboratory.
§ Argonne National Laboratory.

(1) Kresge, C. T.; Leonowicz, M. E.; Roth, W. J.; Vartuli, J. C.; Beck, J. S. *Nature* **1992**, *359*, 710.
(2) Ford, D. M.; Simanek, E. E.; Shantz, D. F. *Nanotechnology* **2005**, *16*, S458–S475.
(3) Wang, Q.; Shantz, D. F. *J. Solid State Chem.* **2008**, *181*, 1659–1669.
(4) Moller, K.; Bein, T. *Chem. Mater.* **1998**, *10*, 2950–2963.
(5) Liu, D.; Zhang, Y.; Chen, C.-C.; Mou, C.-Y.; Poole, P. H.; Chen, S.-H. *Proc. Natl. Acad. Sci. U.S.A.* **2007**, *104*, 9570–9574.
(6) Gutowska, A.; Li, L.; Shin, Y.; Wang, C. M.; Li, X. S.; Linehan, J. C.; Smith, R. S.; Kay, B. D.; Schmid, B.; Shaw, W.; Gutowski, M.; Autrey, T. *Angew. Chem., Int. Ed.* **2005**, *44*, 3578–3582.
(7) (a) Chapman, K. W.; Chupas, P. J.; Kepert, C. J. *J. Am. Chem. Soc.* **2005**, *127*, 11232–11233. (b) Chapman, K. W.; Cupas, P. J.; Maxey, E. V.; Richardson, J. W. *Chem. Commun.* **2006**, 4013–4015. (c) Billinge, S. J. L.; McKimmy, E. J.; Shatnawi, M.; Kim, H. J.; Petkov, V.; Wermeille, D.; Pinnavaia, T. J. *J. Am. Chem. Soc.* **2005**, *127*, 8492–8498. (d) Shatnawi, M.; Paglia, G.; Dye, J. L.; Cram, K. C.; Lefenfeld, M.; Billinge, S. J. L. *J. Am. Chem. Soc.* **2007**, *129*, 1386–1392.

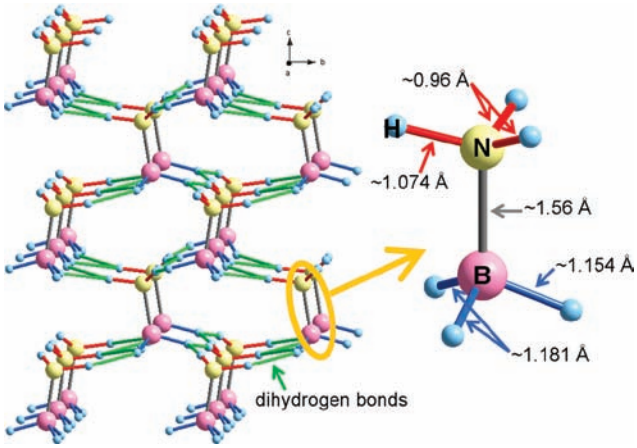

Figure 1. Average crystal structure of neat AB in the orthorhombic phase. Dihydrogen bonds are indicated by green lines to visualize the dihydrogen bonding network. In the tetragonal phase, AB molecules line up along the *c* axis and hydrogen atoms become heavily disordered.

in mesoporous silica MCM-41. Specifically, we have found that heavily loaded AB composite samples contain two different species: one species resides within the mesopores and the other resides outside. The species residing outside the mesopores was not detected in a low loading sample, but it did exhibit Bragg peaks in powder patterns of high loading samples. This suggests that Bragg peaks resulting from the guest may not be always from species *inside* the mesopores. Furthermore, we observed that the low loading of AB and the higher loading of AB in MCM-41 respond to temperature in different ways, suggesting that AB inside and outside the mesopores play different roles in altered properties of this system.

AB has attained considerable attention as a potential material for hydrogen storage. This stable molecular crystal shows promise for achieving high values of both the gravimetric and volumetric densities of hydrogen that would be required for on-board hydrogen storage. In the crystalline solid, highly polarized AB molecules are bound by molecular dipole−dipole interactions and the attractive interactions between the hydridic hydrogen in BH_3 and the protonic hydrogen in NH_3 (Figure 1). The latter interaction is called dihydrogen bonding.[8] Upon heating, the AB solid undergoes an orthorhombic-to-tetragonal phase transition at 225 K. The phase transition is readily observed using X-ray[9] and neutron[10] diffraction, anelastic,[11] Raman,[12] and NMR[13] spectroscopic techniques. At elevated temperatures, hydrogen is released by the series of dehydrocoupling reactions shown below:

$$n\mathrm{NH_3BH_3} \rightarrow (\mathrm{NH_2BH_2})_n + n\mathrm{H_2}$$

$$(\mathrm{NH_2BH_2})_n \rightarrow (\mathrm{NHBH})_n + n\mathrm{H_2}$$

The first reaction occurs below 100 °C (373 K) and the second occurs above 150 °C (423 K). Approximately 15 wt % of hydrogen is released from this material at ~150 °C. Despite the high hydrogen yields, several material challenges must be overcome for AB to be considered viable for fuel cell applications; for example, hydrogen is released (1) at rather high temperatures, (2) after a long induction period, and (3) upon formation of borazine as one of byproducts that affect hydrogen purity.[6]

Recently one compelling approach has been reported to overcome these obstacles—nanocomposition of AB by loading AB in a mesoporous silica material.[6] This outcome is fascinating for several reasons: (1) Faster rates of hydrogen desorption were observed at (2) reduced temperature and (3) the formation of borazine was significantly suppressed. Further study shows that the alteration in AB:MCM-41 properties are highly dependent on the level of AB loading; neat AB-like nature was recovered in high AB loading samples.[14] Even though the improvement is striking, the mechanism responsible for the enhanced properties is not known, in part because of the absence of insight into the structural changes of AB inside mesoporous silica. Conventional crystallographic analysis is not feasible because of its lack of long-range structural order, and transmission electron microscopy (TEM) fails to locate AB guest species because of the low scattering from the light elements compared to the host species (SiO_2). Consequently, there currently is little structural characterization information available. Nevertheless, detailed information on how AB resides in mesoporous channels at different loading levels and how the structure evolves with temperature is critical for understanding the improved properties and furthermore, for designing new materials with optimal hydrogen storage properties.

A recent hyperpolarized (HP) ^{129}Xe NMR study provided a general picture of where supported AB resides in the mesoporous silica host with increases in the loading level.[15] It is evident from the HP ^{129}Xe NMR spectrum that all the AB resides *inside* the mesopores at AB:MCM-41 loading levels of ≤1:2. However, as the loading increases, AB fills the pores completely, and excess AB begins to accumulate outside the pores, forming AB aggregates. This process starts when the AB:MCM-41 level is 1:1. Further loading of AB results in more AB aggregates in the system. While the locality of AB in the mesoporous MCM-41 as a function of loading level was successfully elucidated by HP ^{129}Xe NMR, the structure of AB embedded inside the pores and AB aggregates located outside the pores were not determined.

The structural determination of nanocomposite compounds embedded inside a mesoporous silica host is not straightforward because the materials by definition do not possess long-range structural order. This is especially true for molecules such as AB, which is composed of light elements. Spectroscopic approaches can be sensitive to specific atoms or bonds, however, structural information accessible from such technique is restrained to intramolecular or very first or second nearest neighbors of a specific atom. Usually information of a more extended length scale is not available. An alternative probe often

(8) Crabtree, R. H. *Science* **1998**, *282*, 2000–2001.
(9) Hoon, C. F.; Reynhardt, E. C. *J. Phys. C: Solid State Phys.* **1983**, *16*, 6129–6136.
(10) Hess, N. J.; Schenter, G. K.; Hartman, M. R.; Daemen, L. L.; Proffen, Th.; Kathmann, S. M.; Mundy, C. J.; Hartl, M.; Heldebrant, D. J.; Stowe, A. C.; Autrey, T. *J. Phys. Chem. A* **2009**, *113*, 5723–5735.
(11) Paolone, A.; Palumbo, O.; Rispoli, P.; Cantelli, R.; Autrey, T. *J. Phys. Chem. C* **2009**, *113*, 5872–5878.
(12) Hess, N. J.; Bowden, M. E.; Parvanov, V. M.; Mundy, C.; Kathmann, S. M.; Schenter, G. K.; Autrey, T. *J. Phys. Chem.* **2008**, *128*, 034508.
(13) (a) Penner, G. H.; Chang, Y. C. P.; Hutzal, J. *Inorg. Chem.* **1999**, *38*, 2868–2873. (b) Gunaydin-Sen, O.; Achey, R.; Dalal, N. S.; Stowe, A.; Autrey, T. *J. Phys. Chem. B* **2007**, *111*, 677–681.
(14) Stowe, A. C.; Schmid, B.; Karkamkar, A.; Shaw, W.; Linehan, J. C.; Li, L.; Autrey, T. *Prepr. Pap.-Am. Chem. Soc., Div. Fuel Chem.* **2006**, *5*, 584.
(15) Wang, L.-Q.; Karkamkar, A.; Autrey, T.; Exarhos, G. J. *J. Phys. Chem. C* **2009**, *113*, 6485–6490.

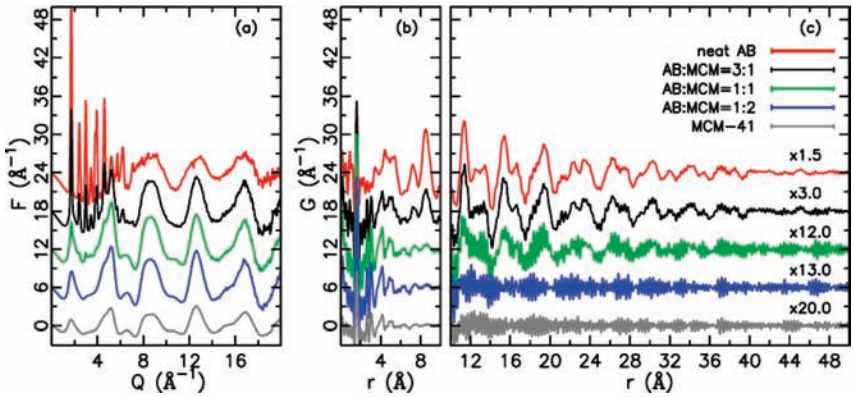

Figure 2. (a) Experimental reduced total scattering structure function, $F(Q)$ and (b) corresponding PDFs for the AB-loaded MCM-41 samples obtained at room temperature. For comparison, data for neat AB and empty MCM-41 are included. (c) $r \geq 10$ Å region of each PDF is shown on an expanded scale to display long-range structural correlation. The scaling factor is indicated above each curve. Both $F(Q)$ and PDFs are offset for clarity.

used for nanoscaled materials is atomic PDF analysis, which is a local structural probing technique that gives the probability of finding atom pairs separated by distance r.[16] It is obtained from a sine Fourier transformation of X-ray or neutron powder diffraction data according to eq 1

$$G(r) = \frac{2}{\pi}\int_0^\infty Q[S(Q) - 1]\sin(Qr)\mathrm{d}Q \qquad (1)$$

where $S(Q)$ is the total scattering structure function and Q is the magnitude of the scattering vector. Because PDF analysis makes use of both Bragg and diffuse intensities and does not require long-range periodicity, it has been widely used[17] to study liquids and amorphous materials and, more recently, to investigate nanocrystalline and disordered materials. The advantage of using PDF analysis as a structural probing technique is that *both local and medium range structural information can be extracted*.

In this study, we applied the PDF analysis of synchrotron X-ray powder diffraction data to elucidate the structural evolution of both AB aggregates and AB embedded inside mesoporous silica as a function of temperature. We found that AB aggregate essentially has the nature of neat AB, which probably plays an important role in the recovery of neat AB-like properties in high AB loading samples. However, AB residing inside mesopores is stabilized in the tetragonal phase at much lower temperatures than neat AB. These results may provide new clues into understanding the rate enhancement of hydrogen release from an AB-loaded MCM-41 system.

Experimental Section

Sample Preparation. The MCM-41 silica materials were purchased from Mobil Corporation. A description of the procedure for preparing AB:MCM-41 = 1:1 samples using a wetness incipient approach follows. A solution of AB (50 mg) in tetrahydrofuran (THF) (1 mL) was added to a sample of MCM-41 (50 mg) in small aliquots. The solution appeared to fill the internal channels of the mesoporous scaffold through capillary action. The "wet" MCM-41 was dried under vacuum to produce a sample with an internal coating of AB (approximately 1:1 AB:MCM-41 by weight). Similar procedures were used for preparing AB:MCM-41 = 1:2 and 3:1 samples using appropriate quantities of AB and MCM-41.

Powder X-Ray Diffraction. Synchrotron X-ray powder diffraction experiments were conducted at the 11-ID-B beamline at the Advanced Photon Source at Argonne National Laboratory. Powder samples of three compositions (with weight ratios of AB:MCM-41 of 1:2, 1:1, and 3:1), as well as neat AB and empty MCM-41, were packed in kapton capillaries with a diameter of 1.0 mm. An incident X-ray energy of 90.486 keV ($\lambda = 0.13702$ Å) was used for collecting room-temperature data of all the samples and low-temperature data of neat AB. To achieve better statistics, all the low temperature data of AB-loaded MCM-41 and empty MCM-41 samples were collected with X-ray energy of 58.26 keV ($\lambda = 0.2128$ Å). For the low-temperature experiments, each sample was cooled to 80 K using an Oxford Cryosystems Cryostream 700, and data were collected at several temperature points during warming to 300 K by using the rapid acquisition pair distribution function (RA-PDF) technique.[18] An amorphous silica area detector manufactured by General Electric Healthcare[19] was mounted orthogonal to the incident beam with a sample-to-detector distance of 221 mm for 90.486 keV and 146 mm for 58.26 keV. A series of frames were collected for each data set to achieve good statistics.[18] Raw data were combined and integrated using the FIT2D software.[20] The signal from an empty container was subtracted from the raw data, and various other corrections were made.[16] The PDF was obtained by a Fourier transformation of $F(Q) = Q[S(Q) - 1]$ according to eq 1 using the PDFgetX2 program.[21] Because of the unfavorable signal-to-noise ratio at high-Q region, $F(Q)$ was truncated at $Q_{max} = 20$ Å^{-1} before the transformation. To reduce the effects of noise at high-Q and termination of $F(Q)$ at Q_{max} each $F(Q)$ was multiplied by a Lorch function.[22] For structural modeling the program PDFgui[23] was used.

Results and Discussion

Evolution of AB as a Function of Loading Level in MCM-41. The reduced total scattering structure functions ($F(Q)$) for the AB-loaded MCM-41 samples obtained at 300 K are shown in Figure 2a and the corresponding PDFs in Figure 2b and c. For comparison purposes, neat AB and empty MCM-41 data are

(16) Egami, T.; Billinge, S. J. L. *Underneath the Bragg Peaks: Structural Analysis of Complex Materials*; Pergamon Press Elsevier: Oxford, England, 2003.
(17) (a) Proffen, Th.; Kim, H. J. *J. Mater. Chem.* **2009**, *19*, 5078–5088. (b) Billinge, S. J. L.; Kanatzidis, M. G. *Chem. Commun.* **2004**, *2004*, 749–760.
(18) Chupas, P. J.; Qiu, X.; Hanson, J. C.; Lee, P. L.; Grey, C. P.; Billinge, S. J. L. *J. Appl. Crystallogr.* **2003**, *36*, 1342.
(19) Chupas, P. J.; Chapman, K. W.; Lee, P. L. *J. Appl. Crystallogr.* **2007**, *40*, 463–470.
(20) Hammersley, A. P.; , S. O. S.; Hanfland, M.; Hauserman, D. *High Press. Res.* **1996**, *14*, 235.
(21) Qiu, X.; Thompson, J. W.; Billinge, S. J. L. *J. Appl. Crystallogr.* **2004**, *37*, 678.
(22) Lorch, E. A. *J. Phys. C* **1969**, *2*, 229.
(23) Farrow, C. L.; Juhas, P.; Liu, J. W.; Bryndin, D.; Božin, E. S.; Bloch, J.; Proffen, Th.; Billinge, S. J. L. *J. Phys.: Condens. Matter* **2007**, *19*, 335219.

shown also, and the curves are offset for clarity. For a low AB loading sample (AB:MCM-41 = 1:2), the features in $F(Q)$ are very broad and similar in appearance to the $F(Q)$ of empty MCM-41. No distinct difference from the silica mesostructure is observed. As the loading level increases, extra features begin to appear on top of the mesoporous silica signal. These features are not substantial, yet they are distinguishable in AB:MCM-41 = 1:1 data. The growth of the features into sharp Bragg peaks is clearly evident in AB:MCM-41 = 3:1 data. Good alignment of the peaks with those found in neat AB strongly indicates the existence of long-range structural order of AB in high AB loading (AB:MCM-41 > 1:1) samples. Comparison of $F(Q)$ data in Figure 2a illustrates that the PDF approach is uniquely apt for investigating nanoconfined guest species in scaffolds, especially at low guest loading levels.

Development of long-range structural order as a function of the AB loading level can be more readily seen in the PDFs (Figure 2(b) and (c)). A distinct feature found in the AB:MCM-41 = 1:2 PDF is a rapid falloff of the PDF profile with increasing r just like one found in the empty MCM-41. This feature reflects the amorphous nature of the silica framework. No significant signal was observed beyond 10 Å (Figure 2c) indicating the absence of long-range structural order of AB at this low loading level. Further loading of AB leads to the development of a new structural feature in the PDF. This is evident from the appearance of a small fluctuation in the AB:MCM-41 = 1:1 curve above 10 Å. It becomes more prominent as additional AB is loaded into the mixture, and becomes well developed at loading levels of AB:MCM-41 = 3:1. The fact that the PDF feature extends to high -r, ~50 Å (Figure 2c) is a strong indication of the formation of long-range structural order of AB. This new *long-range* structural correlation is absent in the AB:MCM-41 = 1:2 sample, barely observable in AB:MCM-41 = 1:1, and clearly evident in the 3:1 samples. Therefore, it most probably results from the *extra* AB aggregating outside the pores as suggested from the HP ^{129}Xe NMR study. The close similarity in PDF peaks of AB:MCM-41 = 3:1 and neat AB beyond 6 Å implies the likeness between the arrangement of AB molecules in AB aggregates and neat AB. Because of the finite instrumental resolution, even the PDF signal of neat AB and a standard crystalline Ni (not shown) completely tapers out at about 50 Å. Therefore, we are unable to determine the size of AB aggregates from current data sets. However, no sample-dependent finite size effect is observed up to 50 Å in AB:MCM-41 = 1:1 and 3:1 data, indicating that the size of the aggregates is much larger than 50 Å.

To determine the structure of AB aggregates, both orthorhombic[24] and tetragonal[25] models of neat AB were used to fit the experimental PDF curves. For comparison, neat AB data also were used for structural refinement. To avoid the MCM-41 signal in the low-r region and noise in the high-r region, a refinement range of $20.0 < r < 50.0$ Å was chosen. A starting model was built using structural information taken from the literature.[24,25] Both atomic coordinates and atomic displacement parameters were fixed, and only lattice parameters were refined until the difference between the experimental and calculated PDFs was minimized. The refined structural parameters are summarized in Table 1, and the results are shown in Figure 3. Both AB:MCM-41 = 1:1 and 3:1 data were more consistent with the tetragonal model than with the orthorhombic model. In addition, the refined orthorhombic models were barely orthorhombic; therefore, we are only reporting the results using the tetragonal model. A reasonably good fit was obtained from the refinement on AB:MCM-41 = 3:1 data (Figure 3). The model explains an overall PDF profile without any marked problem, and the refined lattice parameter values are consistent with the values found for neat AB (Table 1). This finding strongly suggests that at 300 K, the *extra* AB molecules aggregate into the tetragonal structure of neat AB. Similar results were obtained from the data obtained from the AB:MCM-41 = 1:1 sample (Figure 3). The large R_w value is probably the result of noise shown as sharp high-frequency features that can be observed on the difference curves but not observed in the neat AB and AB:MCM-41 = 3:1 data sets. The refinement result for the AB:MCM-41 = 1:2 PDF is shown in the bottom panel of Figure 3. The featureless flat line of the calculated PDF reconfirms the absence of long-range order in this low loading sample at 300 K. Although the refinements of atomic displacement parameters were attempted for all the data, the values did not change.

The absence of the neat AB-like, long-range structural correlations in AB:MCM-41 = 1:2 is consistent with the absence of AB aggregates in this mixture. At this loading level, the HP ^{129}Xe NMR spectrum only shows peaks arising from the empty

Table 1. Refined Structural Parameters Using the Tetragonal Model[a]

	literature[25]	AB	3:1	1:1
a (Å)	5.22814(64)	5.230(3)	5.231(6)	5.23(5)
c (Å)	5.02182(61)	5.022(5)	5.023(9)	5.02(7)
R_w (%)		18.8%	22.3%	62.1%

[a] Only lattice parameters were refined. R_w indicates the degree to which the model fits to data. The refinement range was $20.0 < r < 50.0$ Å.

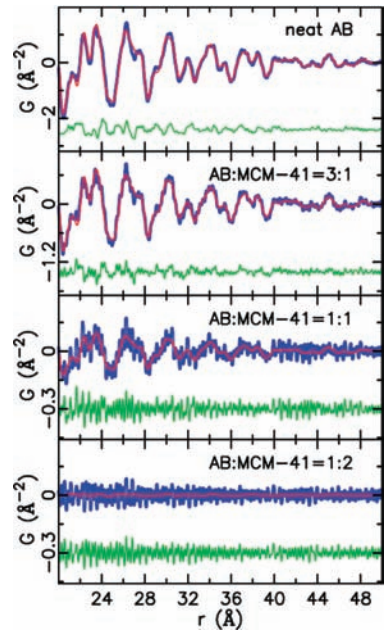

Figure 3. PDF refinement results using the tetragonal model. The experimental PDFs of neat AB, AB:MCM-41 = 3:1, 1:1, and 1:2 are plotted with blue open circles. The red solid line in each panel is the calculated PDF from the corresponding refined tetragonal model. The difference between the measured and calculated PDFs (green solid line) is shifted down for clarity. Note that the results are presented in different expanded scales.

(24) Klooster, W. T.; Koetzle, T. F.; Siegbahn, P. E. M.; Richardson, T. B.; Crabtree, R. H. *J. Am. Chem. Soc.* **1999**, *121*, 6337–6343.
(25) Yang, J. B.; Lamsal, J.; Cai, Q.; James, W. J.; Yelon, W. B. *Appl. Phys. Lett.* **2008**, *92*, 091916.

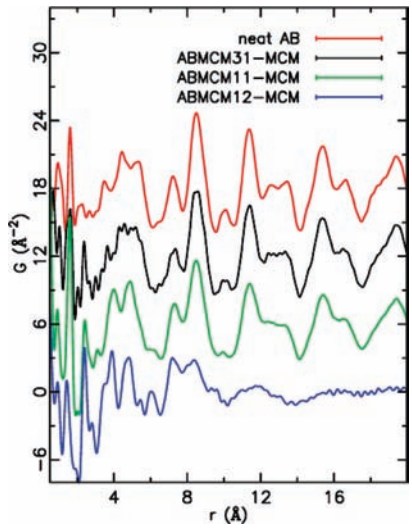

Figure 4. AB-loaded MCM-41 PDFs after the MCM-41 signal was removed. The signal from the MCM-41 host was subtracted from the PDFs of AB:MCM-41 = 1:2, 1:1, and 3:1 (from bottom to top) obtained at 300 K. Resultant PDFs are rescaled to be comparable to neat AB data (top curve). Curves are offset from one another for clarity.

meso-pore channels and channels coated with AB. Therefore, we assumed that by subtracting the empty MCM-41 PDF signal from the AB:MCM-41 = 1:2 PDF signal, we may be able to extract the structural information of AB residing on pore surfaces. Because data with good statistics are essential for this analysis, we used data sets collected for a longer time at 300 K and at an X-ray energy of 58.26 keV. After the empty MCM-41 PDF signal was subtracted, the resulting PDFs were rescaled to be comparable with the neat AB data. The data are presented in Figure 4, and neat AB-like structural features are now seen clearly from AB:MCM-41 = 3:1 and 1:1 data, even below 20 Å. It is worth noting that before subtracting the empty MCM-41 PDF signal, no AB related signal was detected from the high-r region of AB:MCM-41 = 1:2 PDF (Figures 2 and 3), and the low-r region was similar to that of the empty MCM-41. On the other hand, after subtraction, we observed sharp features below 10 Å in the AB:MCM-41 = 1:2 PDF (bottom curve in Figure 4). This is especially evident in the PDF below 6 Å where the peaks are reasonably aligned with those found in AB:MCM-41 = 1:1, *suggesting these sharp features are related to AB located inside mesopores*. A large part of these features are probably from the guest (AB)-host (silica surface) correlation signal because of the large pore surface area. Broad features above 10 Å indicate the disordered nature of AB inside the pores. Analysis of the structural correlation between the AB and the MCM-41 interface was not pursued during this study and is beyond the scope of this paper. However, determining this structural correlation is the topic of a future study.

Structural Evolution As a Function of Temperature. From the analyses of the PDFs of high AB loading samples (AB:MCM-41 = 3:1 and 1:1), the structure of neat AB like aggregates can be determined. On the other hand, even though AB residing *inside* mesoporous channels can be isolated from AB aggregates in low loading samples (AB:MCM-41 ≤ 1:2), the signal is predominantly from the silica frameworks (Figure 2). Hence direct structural modeling on the AB:MCM-41 = 1:2 PDF is difficult. However, we have found that the structural response of AB *inside* pores to temperature is different than the structural response of AB aggregates. This finding provides crucial insight into the structure of nano confined AB. Figure 5 shows the difference between PDFs obtained at two adjacent temperature points. Each difference curve was obtained by subtracting the PDF obtained at high temperature from the PDF obtained at low temperature. The adjacent temperatures associated with each difference are indicated above each curve. Large structural changes are observed from the PDF of neat AB for the 80 K through 200 K temperature range (Figure 5a). This is probably to the result of continuous change in the tilting angle of AB molecules along ***c***-axis.[25] The orthorhombic-to-tetragonal phase transition at 225 K is clearly evident from the curve related to the 220 and 225 K data sets. Despite the 5 K increment in temperature, the structure responds to temperature remarkably well, resulting in a characteristic difference curve. Detailed analysis on temperature-dependent local structural evolution of neat AB will be published elsewhere. As expected, the AB:MCM-41 = 3:1 sample undergoes a structural phase transition at 225 K (Figure 5b), which leads to a similar response curve to one found for neat AB. Notice the close resemblance between the two difference curves (enclosed with a solid red line in Figure 5). In addition, the tetragonal model provides a good fit to data obtained above 225 K but fails to explain data obtained below 220 K (Supplementary Figure 1). AB aggregates are clearly responsible because the same phase transition is absent for the AB:MCM-41 = 1:2 loading (Figure 5c). A close comparison reveals that the structures of neat AB and AB aggregates evolve with temperature basically in a similar manner (same for AB:MCM-41 = 1:1 sample but not shown here) strongly suggesting AB aggregates are very similar to the molecular crystalline AB. This finding explains why neat AB-like hydrogen storage properties are recovered in high AB loading samples where more AB aggregates are observed.[14]

On the other hand, no significant structural modification, including the phase transition at 225 K, was observed from the AB:MCM-41 = 1:2 sample over the temperature range of $110 < T < 240$ K (Figure 5c). The absence of the phase transition at 225 K in the AB:MCM-41 = 1:2 sample and the signature of a little intense transformation in the AB:MCM-41 = 1:1 sample are consistent with recent results from studies that employed differential scanning calorimetry (DSC) and anelastic spectroscopy.[26] However, unique structural alterations occur at temperatures between 80 and 110 K and above 240 K. These structural responses for AB:MCM-41 = 1:2 are not from the MCM-41 host because it does not show any notable change across the whole temperature range (Supplementary Figure 2). In particular, the difference between the 240 and 270 K PDFs contains well-defined features that extend to 40 Å (enclosed with a solid blue line). Beyond that point, no signal was found. Strikingly, these features are indeed characteristic of the neat AB structure in the tetragonal phase. Figure 6 shows how well the difference curve and the PDF of neat AB obtained at 300 K overlap. The structural modeling result using the tetragonal model is shown in Supplementary Figure 3. The structural evolution of AB:MCM-41 = 1:2 can be explained as follows: Below 240 K (possibly down to 110 K because there is no significant change in PDF), AB molecules are arranged in the tetragonal-like structural phase of neat AB inside meso-porous channels. This order extends to many neighbors in the length scale of 40 Å, which is coincidentally approximate to the diameter of pore channels in MCM-41. However, above 240 K, AB loses medium range order. As a result, the difference curve contains the structural correlations that have been lost at

(26) Paolone, A.; Palumbo, O.; Rispoli, P.; Cantelli, R.; Autrey, T.; Karkamkar, A. *J. Phys. Chem. C* **2009**, *113*, 10319–10321.

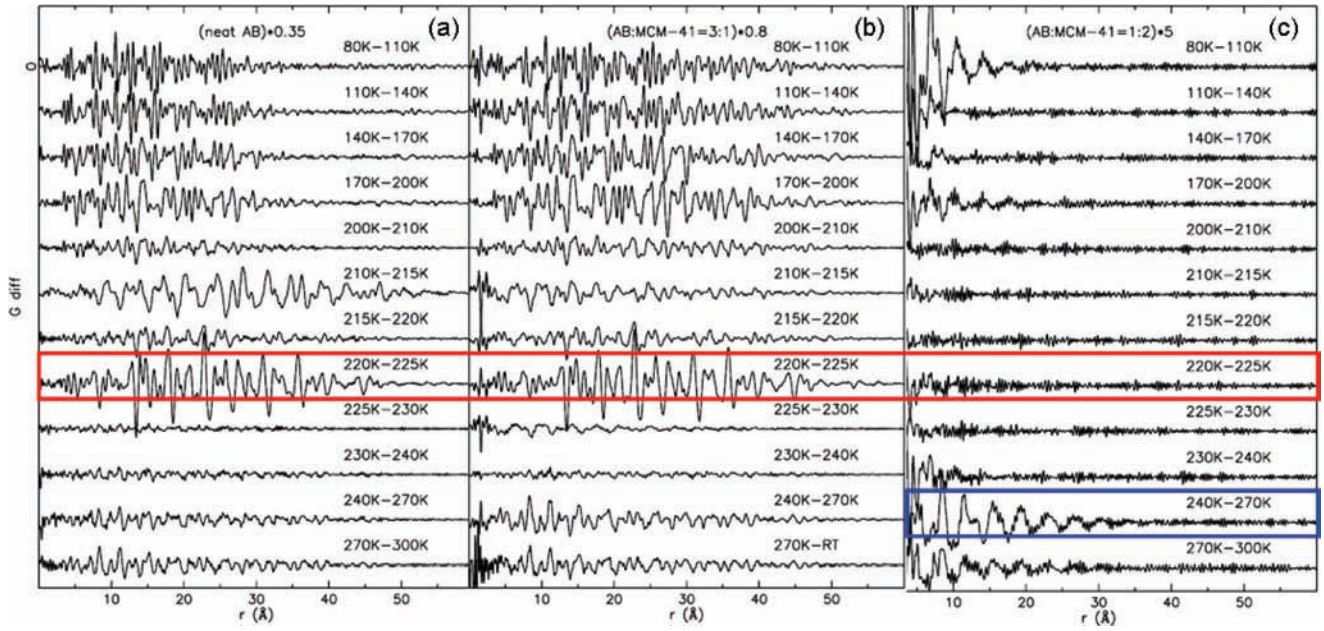

Figure 5. Difference between PDFs obtained at two adjacent temperature points. Each difference curve was obtained by subtracting the high temperature PDF from the low temperature PDF. (a) Neat AB and (b) AB:MCM = 3:1 show similar temperature dependent structural evolution. A red solid line encloses the structural response at the temperature where the orthorhombic to tetragonal phase transition occurs in neat AB. While in high AB loading samples (i.e., AB:MCM-41 = 3:1 and 1:1, but 1:1 is not shown) the phase transition is present, it is clearly absent in (c) the AB:MCM-41 = 1:2 sample. On the other hand, large changes were observed above 240 K in AB:MCM-41 = 1:2, which are obviously not from empty MCM-41 (Supplementary Figure 2). Note that a different scaling factor was used for each sample (i.e., 0.35, 0.8, and 5 for neat AB, AB:MCM-41 = 3:1, and AB:MCM-41 = 1:2, respectively) to make the difference curves comparable. Because a different X-ray energy was used, the signal from AB:MCM-41 = 3:1 extends out to higher-*r* than that from neat AB.

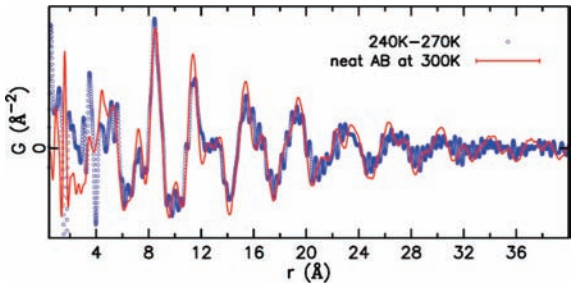

Figure 6. Comparison between the difference in PDFs of AB:MCM-41 = 1:2 at 240 and 270 K (blue open circle) and the PDF of neat AB obtained at 300 K (red solid line). Interestingly, above 5 Å the difference curve overlaps surprisingly well with neat AB data in the tetragonal phase. This finding suggests that below 240 K, AB molecules inside mesopores are arranged in a similar way to the tetragonal structure of neat AB but that structural order is lost at 270 K.

the higher temperatures. From the current set of measurements, we can not define the exact temperature at which the disordering process begins; however, we expect it to be gradual because the change in the structure continues up to 300 K. One potential explanation is that the amorphorization of the AB inside mesopores occurs at a lower temperature than neat AB. This would be consistent with the shorter induction period observed in the hydrogen desorption reaction.[27,28] However, verification of this assumption will require data sets obtained above 300 K. Experiments to obtain these data sets are indeed planned. While the structure of AB inside mesopores turns out to be similar to the structure of neat AB in the tetragonal phase, its structural response to temperature is nonetheless substantially different from that of neat AB. This is a strong indication that the nanocomposition of AB using a mesoporous silica scaffold greatly alters the intermolecular interaction of AB, thus stabilizing the high-temperature tetragonal phase at rather low temperature and likely altering the dehydrogenation properties of AB.

Conclusions

Analyses of the AB:MCM-41 = 1:1 and 3:1 data show that AB aggregates, which are formed by excessive AB that can not become embedded into AB saturate pores, have the tetragonal structure of neat AB at 300 K. Furthermore, there is a close similarity in temperature-dependent structural evolution of the AB aggregates and neat AB, including an occurrence of an orthorhombic-to-tetragonal phase transition at 225 K. This result strongly indicates that AB aggregates and neat AB are very similar. On the other hand, the order−disorder phase transition at 225 K is absent in the AB:MCM-41 = 1:2 sample where all AB is known to reside within the mesopores. Alternatively there is a significant structural change that occurs between 240 and 270 K, perhaps from a crystalline-to-amorphous transition, providing evidence that the nanocomposition of AB inside mesoporous channels of MCM-41 1) stabilizes the tetragonal phase of AB at a much lower temperature and 2) induces a loss of crystallinity at lower temperatures than neat AB. This indicates that intermolecular interaction of AB inside mesopores is altered, and consequently, the dehydrogenation properties of AB are greatly modified. We also have shown how the PDF technique can be used to determine the structure of light element nanocomposites (e.g., NH_3BH_3 in mesoporous silica MCM-41 scaffolds). However, the technique is not limited to this specific system. It can be broadly applied to a wide variety of encapsulated materials as well as organic

(27) Stowe, A. C.; Shaw, W. J.; Linehan, J. C.; Schmid, B.; Autrey, T. *Phys. Chem. Chem. Phys.* **2007**, *9*, 1831–1836.
(28) Bowden, M.; Autrey, T.; Brown, I.; Ryan, M. *Curr. Appl. Phys.* **2008**, *8*, 498–500.

functional groups on mesopore surfaces, thus providing insight into their chemical and physical properties.

Acknowledgment. We thank Valeri Petkov for the preliminary data collection and Evan Maxey, Julianne Coxe, Katharine Page, and Nadine Rademacher for help with the experiments. Work performed at Argonne National Laboratory and use of the Advanced Photon Source was supported by the U.S. Department of Energy, Office of Science, Office of Basic Energy Sciences, under Contract No. DE-AC02-06CH11357. H.K. and T.P. acknowledge support from the Lujan Neutron Scattering Center, funded by the DOE Office of Basic Energy Sciences. Los Alamos National Laboratory is operated by Los Alamos National Security LLC under Contract DE-AC52-06NA25396. T.A. and A.K. acknowledge support from the U.S. Department of Energy, Office of Basic Energy, Division of Chemical Sciences, Biosciences and Geosciences. Pacific Northwest National Laboratory is operated by Battelle for the U.S. Department of Energy.

Supporting Information Available: Structural modeling results on selected data sets and temperature-dependent structural evolution of the empty MCM-41 sample. This material is available free of charge via the Internet at http://pubs.acs.org.

JA904901D